J Mater Sci (2011) 46:4368–4376
DOI 10.1007/s10853-011-5427-6

IIB 2010

Structural investigations on lead-free $Bi_{1/2}Na_{1/2}TiO_3$-based piezoceramics

L. A. Schmitt · J. Kling · M. Hinterstein · M. Hoelzel · Wook Jo · H.-J. Kleebe · H. Fuess

Received: 7 October 2010 / Accepted: 1 March 2011 / Published online: 10 March 2011
© Springer Science+Business Media, LLC 2011

Abstract In this study, recent results from our electron, X-ray, and neutron-diffraction experiments with emphasis on the binary $Bi_{1/2}Na_{1/2}TiO_3$-$BaTiO_3$ (BNT–BT) and ternary $Bi_{1/2}Na_{1/2}TiO_3$–$BaTiO_3$–$K_{0.5}Na_{0.5}NbO_3$ (BNT–BT–KNN) system are presented and contrasted with literature. The experimental results clearly revealed a phase coexistence on the nanoscale level. A systematic study of superlattice reflections in conjunction with microstructural characteristics showed that the BNT-based systems have specific properties in common, which, however, strongly depend on composition. In situ transmission electron microscopy (TEM) electric field experiments unequivocally demonstrated the evolution of lamellar domains. Combining in situ TEM results with published in situ neutron-diffraction experiments, we proposed an electric field-induced phase transition that results in the giant unipolar and bipolar strain observed in specific compositions of the ternary system.

L. A. Schmitt (✉) · J. Kling · M. Hinterstein · M. Hoelzel · W. Jo · H.-J. Kleebe · H. Fuess
Faculty of Materials- and Geo-Sciences, Technische Universität Darmstadt, Petersenstr. 23, 64287 Darmstadt, Germany
e-mail: Ljuba@st.tu-darmstadt.de

M. Hinterstein
Institut für Werkstoffwissenschaften, Technische Universität Dresden, Helmholtzstr. 7, 01069 Dresden, Germany

M. Hoelzel
Research Reactor Heinz-Maier-Leibnitz (FRM II), Lichtenbergstr. 1, 85747 Garching b. Munich, Germany

Introduction

For the last few decades, lead-containing ceramics such as $Pb(Zr_{1-x}Ti_x)O_3$ (PZT)-based systems have been the material of choice for actuator, sensor, and transducer applications due to their superior dielectric, piezoelectric, and mechanical properties. Environmental regulations [1, 2] are the major driving force in the search for lead-free piezoceramics, which are considered a potential substitute for PZT. An overview of recent developments on lead-free systems considering the mechanical properties is given by several authors [3–12]. Key parameters of applicable materials are piezoelectric coefficients, relative permittivity, electric field-induced strain, and the electromechanical coupling factor.

Although numerous investigations have been presented for lead-free ferroelectrics and piezoceramics, an overview, which focuses on the structural aspect of these materials, is still rare. Hence, this overview summarizes and discusses recent results of our transmission electron microscopy (TEM), X-ray powder diffraction (XRD), and neutron-diffraction investigations, focused on $Bi_{1/2}Na_{1/2}TiO_3$ (BNT) as well as the binary $Bi_{1/2}Na_{1/2}TiO_3$–$BaTiO_3$ (BNT–BT) and ternary $Bi_{1/2}Na_{1/2}TiO_3$–$BaTiO_3$–$K_{0.5}Na_{0.5}NbO_3$ (BNT–BT–KNN) system.

Experimental

For this study, ceramics of the binary $(Bi_{1/2}Na_{1/2}TiO_3)_{0.94}$–$(BaTiO_3)_{0.06}$ and ternary system $(Bi_{1/2}Na_{1/2}TiO_3)_{1-x-y}$–$(BaTiO_3)_x$–$(K_{0.5}Na_{0.5}NbO_3)_y$ were chosen. For simplicity-tested compositions are abbreviated with the relative content of the constituents, e.g., $(Bi_{1/2}Na_{1/2}TiO_3)_{0.90}$–$(BaTiO_3)_{0.07}$–$(K_{0.5}Na_{0.5}NbO_3)_{0.03}$ is abbreviated as 90-07-03. Samples

90-07-03, 91-03-06, 92-06-02, and 94-05-01 were analyzed by electron diffraction. Samples 90-07-03, 91-06-03, 91-07-02, 92-06-02, 92-07-01, 93-05-02, 93-06-01, and 94-05-01 were analyzed by X-ray and neutron diffraction. Furthermore, an in situ TEM experiment applying an external electric field was performed on sample 91-06-03.

Samples were synthesized using the conventional solid-state sintering method from Bi_2O_3, Na_2CO_3, $BaCO_3$, TiO_2, K_2CO_3, Na_2CO_3, and Nb_2O_5 powders. Further information on specimen synthesis is given in Zhang et al. [13].

For TEM investigations, samples were prepared by a standard ceramographic technique such as polishing, disc cutting, and subsequent ion milling. Detailed information on TEM specimen preparation can be obtained from Schmitt et al. [14, 15]. The experiments were performed with a CM20 (FEI, Eindhoven, the Netherlands), operated at 200 keV.

In situ electric field experiments were conducted at the Department of Materials Science and Engineering, Iowa State University, Ames with a CM30 (FEI, Eindhoven, the Netherlands). Technical specifications of the experimental setup are reported by Kling et al. [16].

High-resolution X-ray diffraction was carried out at the powder diffraction beamline MS at the Swiss Light Source (SLS, Villigen, Switzerland) with an incident wavelength of $\lambda \approx 0.4433$ Å ($\approx$28 keV) [17]. Data were recorded utilizing a position-sensitive microstrip detector [18]. The wavelength and the instrumental profile were determined with an Al_2O_3 standard (SRM NIST 676a). Neutron powder diffraction measurements were carried out on the SPODI powder diffractometer at the research reactor FRM-II (Garching b. Munich, Germany) [19] with an incident wavelength of 1.548 Å. Data were collected by a bank of 80 position-sensitive 3He-detectors covering a 160° scattering range. The wavelength and the instrumental profile were determined with a silicon (SRM NIST 640c) and a corundum standard, respectively.

Full-profile Rietveld refinement was performed using the software package FULLPROF [20]. The peak profile shape was described by a pseudo-Voigt function [21]. The diffraction pattern background was fitted using the linear interpolation between selected data points in non-overlapping regions. Scale factor, lattice parameters, atomic positions, isotropic displacement factors, and zero angular shift were varied during the refinement.

Single compound $Bi_{1/2}Na_{1/2}TiO_3$ as a base composition

The base composition $Bi_{1/2}Na_{1/2}TiO_3$ (BNT) is considered to be an excellent lead-free piezoceramic due to its high remanent polarization of 38 $\mu C/cm^2$ [9].

Previous neutron powder diffraction studies on BNT at 698 K, performed by Jones and Thomas [22, 23] reveal a tetragonal P4bm structure, which is composed of in-phase tilts of oxygen octahedra combined with unusual anti-parallel displacements of cations along the polar c axis [22]. Furthermore, Rietveld neutron powder analyses in the temperature range of 5–873 K revealed two temperature-dependent phase transitions. Between 5 and 593 K the phase is rhombohedral (R3c). At 593 K, the tetragonal P4bm phase was observed [23]. Above 813 K, the cation displacements disappeared, showing the ideal cubic paraelectric structure. A broad region of coexistence of the rhombohedral and tetragonal phase was found between 528 and 673 K [23].

Contrary to Jones and Thomas [23], Dorcet and Trolliard [24, 25] observed a phase coexistence even at room temperature with TEM. They observed ½{ooo} and ½{ooe} superlattice reflections, where o and e denote odd and even Miller indices, respectively. They proposed a coexistence of two types of octahedral tilt systems, namely $a^-a^-a^-$ and $a^0a^0c^+$ (Glazer notation) [26]. They suggested that the microstructure consists of tetragonal platelets, exhibiting three different orientation variants within a rhombohedral matrix. In the $[100]_c$ zone, ½{oee} superlattice reflections were detected during hot-stage experiments by Dorcet et al. [25, 27]. They suggested the occurrence of an intermediate orthorhombic Pnma phase between 473 and 593 K, periodically separating layers of R3c structure. At about 593 K, a second order transition to a tetragonal phase occurs [27]. At 893 K, ½{ooo} and ½{ooe} superlattice reflections were still visible. They suggested that a small amount of tetragonal and rhombohedral domains is still present, embedded in the cubic phase.

A recent high-resolution X-ray diffraction study of a $Bi_{1/2}Na_{1/2}TiO_3$ single crystal, undertaken by Gorfman and Thomas [28], revealed that the average structure has lower than rhombohedral symmetry. Thereby in each case, single phase (tetragonal, orthorhombic, and rhombohedral) as well as multi phase (rhombohedral + tetragonal and rhombohedral + orthorhombic), least-square fits of the splitting in 2θ were performed. Best fits were achieved for either monoclinic solutions or a combination of rhombohedral + tetragonal or rhombohedral + orthorhombic lattice symmetry. Moreover, they observed weak $\{½\ ½\ ½\}_{pc}$ reflections in the *hhl* sections of the reciprocal space, which are forbidden in space group R3c. This evidence confirmed the presence of a C-centered monoclinic cell. An additional 180° ω-rocking curve of the ½ ½ ½ reflection, collected during rotation around the [111] reciprocal lattice direction, revealed that the additional reflection, considered as evidence for the existence of a Cc phase, was due to double diffraction. Hence, the presence of this reflection cannot exclusively be used as proof for the presence of monoclinic symmetry.

Diffuse X-ray scattering experiments revealed displacements of the Na^+ and Bi^{3+} ions away from the rhombohedral <111> direction toward tetragonal <100>, resulting in a local monoclinic symmetry [29]. From this study, Kreisel et al. [29] suggested the existence of narrow plate-like-shaped monoclinic regions. Their studies were supported by Cordero et al. [30], who, based on anomalies observed during anelastic and dielectric measurements, proposed a locally monoclinic symmetry in BNT–BT ceramics.

However, despite the large remanent polarization, the usability of BNT in piezoelectric devices is limited by the large coercive fields of about $E_c = 7.3$ kV/mm and high electrical conductivity at room temperature [8, 9, 31–34]. To improve piezoelectric properties of BNT, doped binary and ternary BNT-based systems were studied by several research groups [9, 32–38]. Among the numerous systems, BNT–BT and BNT–BT–KNN systems are considered as appropriate candidates due to their superior piezoelectric properties [7, 13, 38–40], which is based on the existence of a so-called morphotropic phase boundary (MPB). Structural aspects of both systems will be discussed in the following two sections.

Binary system $(1 - x)Bi_{1/2}Na_{1/2}TiO_3$–$xBaTiO_3$

Since there is always the question of cation ordering in these kind of materials, an approach to combine high-resolution transmission electron microscopy (HRTEM), HRTEM image simulation and density functional theory (DFT) were chosen to verify this in 94-06-00 [41]. Supercells with different cation ordering on the A-site were built up and relaxed by DFT calculations. HRTEM image simulations were performed from these structures and compared to experimental HRTEM images. As a result, the most probable structure did not exhibit preferred A-site cations on specific sites. Therefore, no cation ordering is assumed. Areas of different contrast in the HRTEM image could be attributed to slightly misoriented crystal regions with respect to the overall orientation.

This finding supports the model of randomly oriented nanometer-sized regions observed by Ma and Tan [42]. They suggested a possible existence of randomly oriented antiferroelectric nanodomains, which are mirrored as a frequency dispersion in their dielectric measurements. This is in agreement with observations by Ge et al. [33] on a 92-08-00 single crystal. A distinct correlation between domain structure and dielectric constant was observed by Ma and Tan [42]. Combining the results of the macroscopic and microscopic measurements, a phase diagram of the binary BNT–BT system between $x = 0.04$ and 0.12 was constructed. Highest piezoelectric properties were measured at the MPB separating a ferroelectric R3c and a "relaxor antiferroelectric" P4bm phase at $x = 0.06$, while the compositions with $0.07 \leq x \leq 0.10$ showed only the existence of a P4bm phase and the absence of depolarization temperature. They proposed the concept of a "relaxor antiferroelectric" material. For $x \geq 0.11$, a phase transition to P4 mm was reported, supported by the absence of superlattice reflections. A high volume fraction of large lamellar ferroelectric domains observed by TEM coupled with a minimum frequency dispersion of the dielectric behavior was also reported for this material.

Regarding the MPB composition, comparable results were previously reported by Takenaka et al. [32]. Based on the X-ray diffraction, a rhombohedral–tetragonal morphotropic phase boundary (MPB) near $x = 0.06$–0.07 was proposed. A composition dependent transformation from the rhombohedral phase for $x < 0.06$ to the tetragonal phase for $x > 0.07$ with a coexistence region at $x = 0.06$–0.07 occurs. Polarization hysteresis loops for 95-05-00 revealed a large remanent polarization of about 20 $\mu C/cm^2$ at room temperature. Increasing the temperature to 433 K, a pinched loop without remanent polarization was observed leading to the conclusion that a temperature-dependent transition to an antiferroelectric phase proceeded. With X-ray diffraction, Ranjan and Dviwedi [43] confirmed a rhombohedral to pseudocubic phase transition with increasing x. The structure was described as pseudocubic for $x \geq 0.06$.

Zhang et al. [39] studied the temperature-dependent electrical properties of 94-06-00 ceramics. Polarization and strain measurements showed that a dominant ferroelectric order persists up to about 373 K, featured by a typically ferroelectric polarization–electric field P(E) loop with $P_{max} = 40$ $\mu C/cm^2$ and a butterfly bipolar strain–electric field curve S(E), showing a negative strain of about 0.1%. When the temperature was increased to 373 K, the P(E) loop was pinched and the S(E) curve showed the maximum total strain of about 0.4%, while the negative strain vanished. They ascribed this behavior to a ferroelectric to antiferroelectric phase transition in reference to Takenaka et al. [32]. Though the proposed antiferroelectric order is still a controversial [44] we keep this terminology as long as it is specifically mentioned in the references.

In spite of the controversies over the structure of 94-06-00, it is clear that from the microscopic point of view, both types of superlattice reflections were observed in 94-06-00 ceramics by TEM, as depicted in Fig. 1. This sample was also used for the HRTEM analysis reported by Kling et al. [41]. A bright field (BF) micrograph is shown in Fig. 1a. A grainy contrast is visible, which is representative for the entire sample. The corresponding diffraction pattern along the $[110]_c$ zone is depicted in Fig. 1b. Superlattice reflections of type ½{ooo} are visible, marked with an arrow. In Fig. 1c, a diffraction pattern along $[100]_c$ is shown, taken

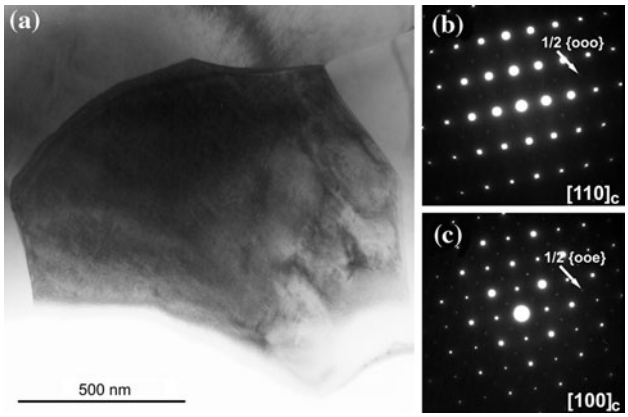

Fig. 1 **a** Bright field (BF) micrograph of sample 94-06-00 showing a fine grainy morphology, which is representative for the whole sample. This sample was also used for the HRTEM study published in Kling et al. [41]. **b** corresponding $[110]_c$ zone axis diffraction pattern. The ½{ooo} superlattice reflections are weakly excited. **c** diffraction pattern taken from a neighbor grain along [100]. ½{ooe} superlattice reflections are visible

from an adjacent grain. Superlattice reflections of type $h = 1$ are excited due to double diffraction.

In general, possible mechanisms for the formation of superlattice reflections are (I) chemical ordering of either A- or B-site cations, (II) antiparallel displacements of ions, or (III) tilting of oxygen octahedra [45, 46].

Soukhojak et al. [46] investigated the temperature-dependent structure of tetragonal 92-08-00, rhombohedral 97-03-00, and pure BNT ceramic with SAED and bright field TEM. Domain morphology present at room temperature gradually disappeared on heating to about 473 K and re-established reversibly upon cooling. SAED revealed that all three compositions exhibited ½{ooe} superlattice reflections at room temperature, even though the intensity of superstructure reflections increased with increasing $BaTiO_3$ content. They suggested octahedral tilting as the most probable origin of the superlattice reflections. Chemical ordering of cations was rejected by them due to the experimental observation that the superlattice was completely restored during rapid cooling from 973 K. Similarly, they discarded the mechanism of anti-parallel displacements of ions. According to Park et al. [47] this should lead to dielectric anomalies at temperatures above 613 K, which was not observed.

Regarding device operation, depolarization temperature is one of the most important parameters for engineering lead-free piezoceramics, since a remarkable enhancement of piezoelectric properties is simultaneously accompanied by a strong reduction in depolarization temperature [9]. For ternary systems, which will be presented in the next section, Zhang et al. [38, 40] showed that the depolarization temperature strongly depends on composition. For compositions exhibiting ferroelectric character, the depolarization temperature is in general higher than for materials with mixed ferroelectric, antiferroelectric, or non-polar phases.

Ternary system $(1 - x - y)Bi_{1/2}Na_{1/2}TiO_3$–$xBaTiO_3$–$yK_{0.5}Na_{0.5}NbO_3$

Because of their outstanding properties, e.g., giant recoverable strain (0.45%), lead-free systems containing $(Bi_{1/2}Na_{1/2})TiO_3$ (BNT), $BaTiO_3$ (BT), and $K_{0.5}Na_{0.5}NbO_3$ (KNN) are promising alternative candidates for actuator applications [13, 38, 40].

Preliminary investigations on $(Bi_{1/2}Na_{1/2}TiO_3)_{1-x-y}$–$(BaTiO_3)_x$–$(K_{0.5}Na_{0.5}NbO_3)_y$ by Zhang et al. [13, 38, 40] focused on an array of nine compositions, with $x = 0.05$–0.07 and $y = 0.01$–0.03. Interestingly, the examined compositions exhibited significantly different piezoelectric properties. Based on strain measurements, Zhang et al. [40] categorized the analyzed piezoceramics into two groups. Group I compositions exhibit a dominant ferroelectric order, whereas group II compositions show a mixed weak ferroelectric and antiferroelectric order. The maximum strain reached up to 0.45% for sample 92-06-02. This giant strain was at first attributed to a field-induced antiferroelectric-ferroelectric phase transition [13, 40], but has been more recently ascribed to a field-induced non-polar-to-ferroelectric phase transition by Jo et al. [48]. Our TEM studies focused on specimen 90-07-03, which exhibits non-polar behavior, samples 91-06-03 and 92-06-02, which both have mixed non-polar and ferroelectric properties, and composition 94-05-01, which possesses ferroelectric order.

In a detailed TEM study, the coexistence of the rhombohedral R3c and the tetragonal P4bm phase within individual grains in the 91-06-03 system was observed [14]. Similar observations were reported by Ma and Tan for specimen 94-06-00 [42]. A distinct correlation between superstructure reflections of the SAED pattern and the excited area in the dark field (DF) image was confirmed. The coexistence of both phases on the nanoscale was verified. The tetragonal phase showed lamellar-nanosized platelets, whereas the rhombohedral phase showed clear domains of {100} and {110} edge-on oriented planes.

A comparative study, comprising X-ray, neutron, and electron diffraction was conducted on specimen 92-06-02 and 94-05-01 [15]. TEM and powder diffraction experiments revealed the presence of a rhombohedral R3c and a tetragonal P4bm phase. Superlattice reflections were employed to identify the rhombohedral and tetragonal phase.

Rietveld refinement on 92-06-02 revealed a low spontaneous polarization of $P_s = 3.4\ \mu C/cm^2$ and a small octahedral tilting angle. The analyses of lattice parameters and atomic positions from powder diffraction data revealed the weak-polar nature of P4bm. The antiparallel atomic

displacements result in an almost extinction of the dipole moment. Together with the pseudocubic lattice symmetry, this phase can be characterized as being non-polar.

With high-resolution neutron diffraction [15], ½{ooe} superlattice reflections (with $h \neq k$) were observed for all investigated compositions attributed to the existence of in-phase tilting of oxygen octahedra. According to Glazer notation [26] this tilt can be specified as $a^0a^0c^+$ tilting. All three tetragonal orientation variants, displayed as ½{ooe} superlattice reflections in the $<111>_c$ zone, were observed [14, 15], leading to the conclusion that tetragonal plate-like regions coexist on a nanoscale. Dorcet and Trolliard [24] also observed this phenomenon in pure $Bi_{1/2}Na_{1/2}TiO_3$. Compared to the pseudocubic reflections of the neutron and X-ray data, the tetragonal superlattice reflections were broadened significantly due to a short-range order of the octahedral tilting. This is consistent with the streaking of ½{ooe} superlattice reflections observed by electron diffraction [14].

In Fig. 2, bright field (BF) micrographs of sample (a) 90-07-03, (b) 92-06-02, and (c) 94-05-01 are shown. Sample 90-07-03 (Fig. 2a), belonging to group II ferroelectrics [40], reveals a grainy morphology with a high amount of non-polar tetragonal phase.

In Fig. 2a and b, a grainy morphology is visible. Within the grains exclusion-like areas of several 100 nm (marked with arrows) with lamellar domain contrast were frequently observed. The inset shows the corresponding selected area electron diffraction pattern (SAED) along the $[111]_c$ zone. Strongly excited ½{ooe} superlattice reflections are visible, showing streaking along the [112] direction. This is due to a short-range order of tilted oxygen octahedra. Also for the P4bm phase, $h = k$ reflections are visible due to double diffraction. The grain morphology of specimen 94-05-01 is depicted in Fig. 2c. The major fraction of the sample consists of domain-like regions, which can be related to a higher rhombohedral phase fraction [15]. The inset shows the SAED pattern, which reveals weakly excited ½{ooe} superlattice reflections. In Fig. 2d–f, the corresponding SAED patterns along $[112]_c$ are depicted. In this zone axis, both types of superstructure reflections are visible. For a better comparability SAED images were not rotated with respect to the BF image.

In specimen 94-05-01 (Fig. 2f), the ½{ooo} superstructure reflections are strongly excited, whereas the ½{ooe} ones are scarcely visible. X-ray and neutron-diffraction analyses of specimen 94-05-01 revealed generally the existence of a rhombohedral phase [15], which in comparison to 92-06-02, is significantly distorted. Higher indexed reflections clearly showed a two-phase coexistence. The observed ½{ooo} superlattice reflections originate from anti-phase tilting of oxygen octahedra, which

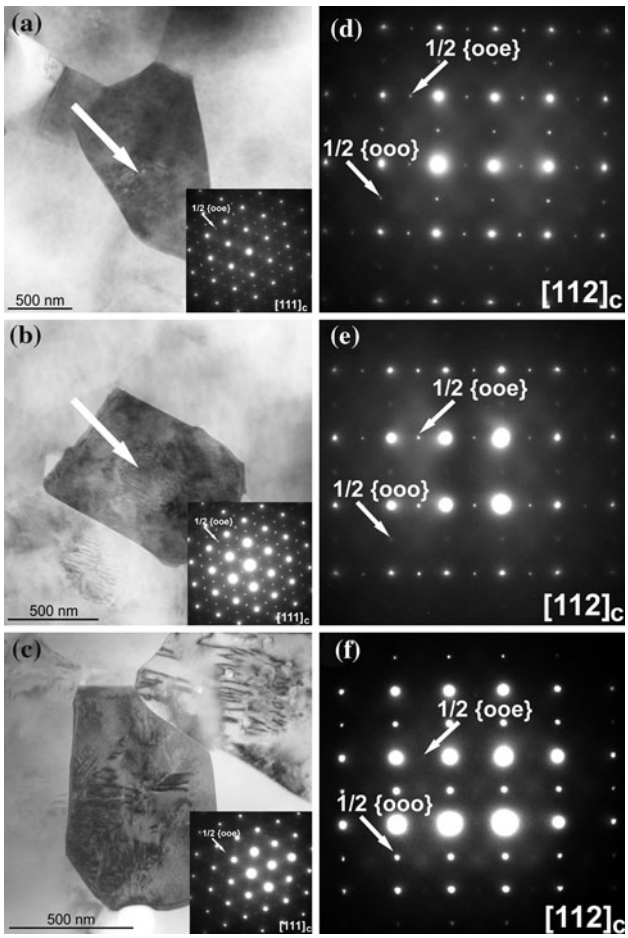

Fig. 2 Bright field (BF) micrographs of sample **a** 90-07-03 and **b** 92-06-02 showing a grainy morphology. Within the grains exclusion-like areas (*marked with arrows*) with lamellar domain contrast are visible, which were frequently observed. The *insets* show the corresponding selected area electron diffraction patterns (SAED) along $[111]_c$ zone. Strongly excited ½ {ooo} superlattice reflections are visible. **c** BF picture of specimen 94-05-01. The major fraction shows domain-like regions. The *inset* shows the SAED pattern, which reveals weakly excited ½ {ooe} superlattice reflections. SAED patterns along [112] zone axis for **d** composition 90-07-03, **e** 92-06-02, and **f** 94-05-01. Superlattice reflections ½ {ooo} and ½ {ooe} are marked with white arrows. **d** and **e** samples 90-07-03 and 92-06-02 show strong ½ {ooe} and weak ½ {ooo} superstructure reflections. Contrary to that **f** sample 94-05-01 exhibits strong ½ {ooo} and very weak ½{ooe} superstructure reflections

can be described by the Glazer [26] notation as $a^-a^-a^-$ for R3c phase.

With neutron powder diffraction ½{ooe} superlattice reflections with $h \neq k$ were found in all investigated compositions, whereas ½{ooo} superlattice reflections with $h \neq k$, $k \neq l$, $h \neq l$ were only found on the rhombohedral side [15]. Figure 3 depicts the ½{310} and ½{311} reflections for $y = 2$ (Fig. 3a) and $x = 6$ (Fig. 3b). The only significant intensity of the ½{311} reflection was observed in 93-05-02 and 94-05-01 [15]. High-resolution

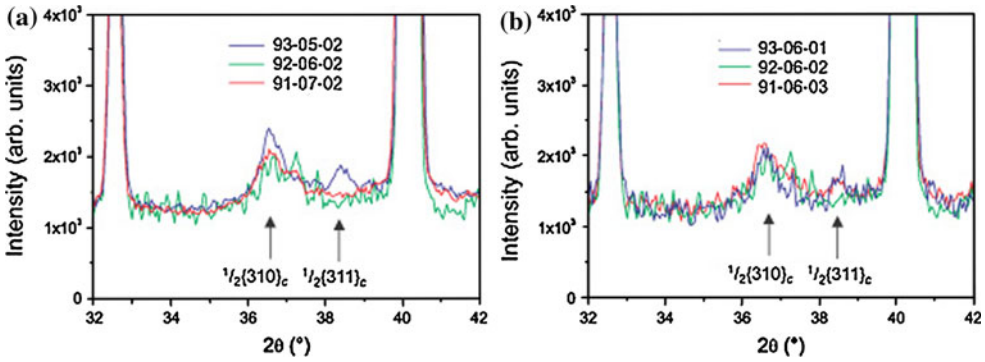

Fig. 3 Comparison of the ½{310} and ½{311} reflections for **a** constant KNN content and **b** constant BT content by neutron-diffraction data

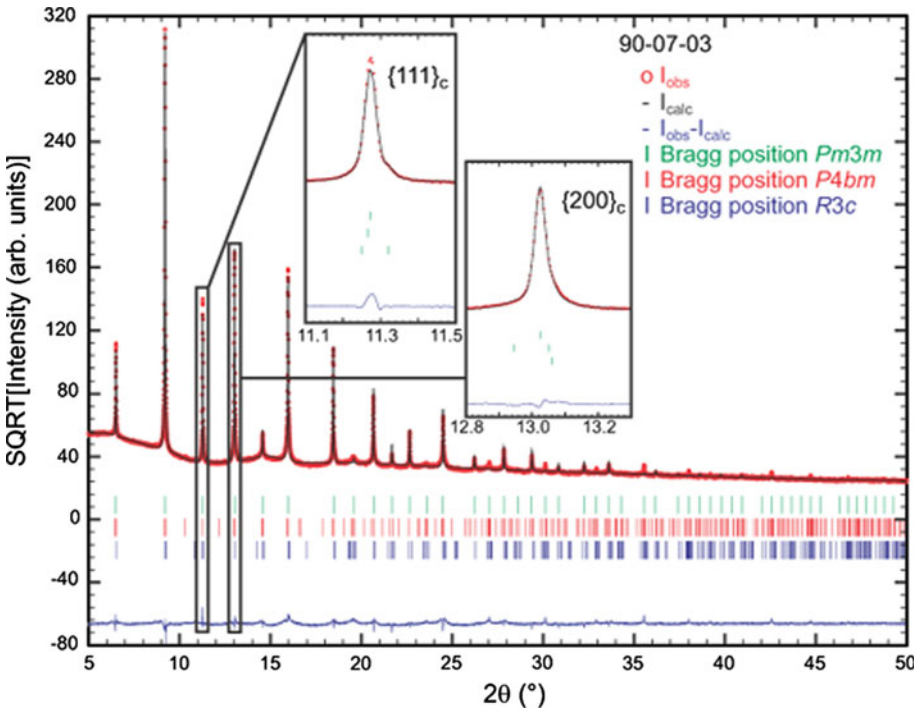

Fig. 4 X-ray diffraction pattern of sample 90-07-03. The model for Rietveld refinement comprised three phases. As a result a phase fractions of 80% cubic Pm-3m, 17% tetragonal P4bm and 3% rhombohedral R3c phase were obtained. The *inset* shows the 111 reflection exhibiting weak rhombohedral shoulders and 200 reflection with even weaker tetragonal shoulders

X-ray diffraction is not sensitive enough to the oxygen matrix to give sufficient intensity for those superlattice reflections. Nevertheless, the high angular resolution and good signal to noise ratio revealed small volume fractions of distorted phases in the pseudocubic matrix (Fig. 4). The reflections of the distorted phases are significantly broadened. Due to their low intensity, a microstructural analysis is not feasible and thus the influence of strain and size effects cannot be quantified. However, since TEM shows rhombohedral and tetragonal superlattice reflections, whereas neutron diffraction does not, it is likely that the distorted phases exist on a local scale. These small distorted areas additionally cause microstrains in the surrounding pseudocubic matrix. Therefore, a significant broadening of the observed reflection results. A careful refinement with a three-phase model of a cubic, a tetragonal, and a rhombohedral phase is expected to give insight in the complex phase composition of the investigated samples. There is, however, no straightforward correlation between phase composition and resulting piezoelectric properties.

Figure 5 depicts the range of the investigated compositions in the ternary phase diagram. The corresponding volume fractions of the three different phases are symbolized by a pie chart for each investigated composition. The most pronounced structural changes occurred in the composition (x) range when KNN content was 1 mol.%. As already implied by the superlattice reflections, volume fractions of distorted tetragonal phase can be found in all compositions. With increasing x, the volume fraction of distorted rhombohedral phase decreases to a value close to the resolution limit for $x \geq 6$. The two compositions with the highest field-induced strain, 91-06-03 and 92-06-02, have the lowest volume fraction of distorted tetragonal

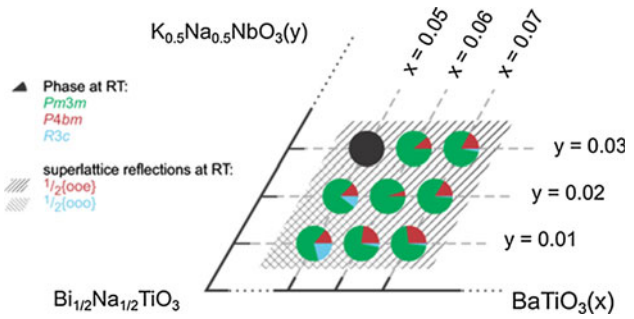

Fig. 5 Investigated compositions of the ternary phase diagram. Volume fractions are presented as pie charts for each investigated composition. All analyzed samples exhibited a distorted tetragonal phase, even though with different amount. Lowest volume fractions of distorted tetragonal phase and no evidence for a distorted rhombohedral phase were observed for 91-06-03 and 92-06-02. Highest amount of rhombohedral phase was determined for sample 94-05-01

phase and no evidence for a distorted rhombohedral phase. This confirms the theory that the giant strain is a result of a reversible field-induced phase transition from a pseudocubic non-polar phase to a ferroelectrically active rhombohedral phase [48, 49], which is most pronounced for compositions at the boundary between group I and group II ferroelectrics.

The R3c phase in general exhibits a ferroelectric character. The highest amount of R3c phase was observed for sample 94-05-01, a representative sample of group I compositions [40], exhibiting dominant ferroelectric character. The results indicate a composition dependent phase transition from a predominantly non-polar phase in 90-07-03 to a ferroelectrically active phase in 94-05-01.

Apart from temperature and composition driven phase transitions [32, 46], the application of an external electric field can result in a similar response [16, 36].

Figure 6a shows an overview of the sample before applying any field. Only a weak contrast within and between the grains is visible. Formation of domains under an applied electric field was monitored within an in situ electric field TEM experiment on composition 91-06-03 depicted in Fig. 6b. A voltage of ±500 V was applied leading to a nominal electric field strength of ±2.5 kV/mm. Depending on electrode geometry and sample morphology, the actual field in the electron transparent regions can reach values of about ±5 kV/mm [16, 50]. Under applied electric field, the evolution of lamellar domains was observed within several grains. The visibility of domains was dependent on the crystallographic orientation. Figure 6c shows the grain morphology after the application of an external electric field. A grainy contrast is visible, comparable with the contrast before electric field application. Concerning the evolution of superstructure reflections, no pronounced changes were observed. Both superstructure

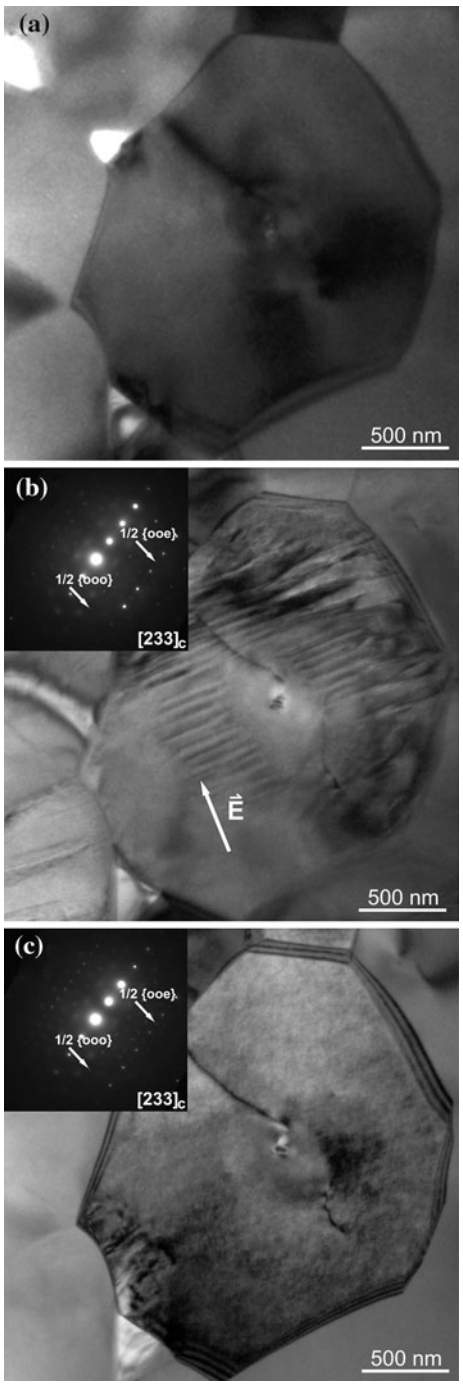

Fig. 6 Sample 91-06-03 was chosen for in situ TEM electric field experiment. **a** BF micrograph showing one grain prior to electric field application. A grainy contrast is visible. **b** BF micrograph showing one grain under an applied electric field at nominal –2.5 kV/mm. Actual field at the area under examination can reach values of about ±5 kV/mm [16, 50]. Formation of lamellar domains is visible. The *inset* shows the SAED pattern. The grain was oriented along $[233]_c$ direction, where both superstructure reflections are visible (*marked with arrows*). **c** removing the electric field the visible domain configuration vanishes, leading to the grainy contrast comparable to the contrast prior to application of an electric field. Both superstructure reflections are visible in the SAED pattern shown in the *inset*

reflections are present before and remain under as well as after electric field application. Quite similar results were observed for composition 92-06-02. A detailed study concerning the reaction of the sample to an applied electric field is given by Kling et al. [16] for the 91-06-03 system. Comparing this structural transition with polarization and strain hysteresis measurements [16], we could monitor a clear indication for a phase transition from non-polar-to-ferroelectric phase and vice versa.

Consistent with the current observations, neutron-diffraction experiments on 92-06-02 conducted by Hinterstein et al. [49] under an applied electric field showed the appearance of ½{ooo} superlattice reflections. We suggest that the initial minor rhombohedral phase, represented as exclusion-like areas within the grains [14], thereby acts as a nucleation site during electric field-induced phase transformation. This response indicates a strong analogy to the polar nanoregions in relaxor ferroelectrics. The initial structure exhibits a pseudocubic matrix with short-range ordering of the octahedral tilting and lattice displacements on the local scale. This non-polar matrix represents the precursor for the ferroelectrically active rhombohedral phase. Therefore, the pinched shape in the P(E) curves with traces of remanent polarization during bipolar cycling, as reported by Jo et al. [48], are very likely to originate from such relaxor-like behavior.

Conclusion

- Depending on temperature and processing route different phases were observed by various researchers, indicating that the phases formed are strongly dependent on processing parameters. Therefore, results from different investigators need to be compared with great caution. Nevertheless, the BNT-based materials seem to have several aspects in common, like the phases present and comparable microstructure.
- In the search for new lead-free piezoceramics, key parameters such as Curie temperature, depolarization temperature, remanent polarization, coercive field, dielectric constant, and electromechanical coupling factor have to be taken into account. Thereby, structural aspects like a possible composition, temperature, or electric field triggered phase transformations have to be considered as well.
- Combined macroscopic (strain, polarization, and dielectric constant) and microscopic studies (electron-, X-ray-, and neutron diffraction) lead to the conclusion that the observed microstructure is closely related to the present phases and phase fractions of the analyzed material.
- Evolution of microstructure and structure on an atomic scale is conditioned by several parameters. Therefore, this interplay of several parameters makes a prediction about the response of the system challenging.
- Subtle changes in A-site and B-site occupancy by means of one of the four different A-site cations and two for the B-site influence the phase fractions remarkably.
- Our combined HRTEM and DFT study on 94-06-00 [41] revealed a homogeneous A-site occupation, exhibiting no specific chemical ordering. Different contrast in HRTEM images could be attributed to a slight tilting of the structure, restricted to nanometer-sized regions.
- Phase coexistence was evidenced by means of TEM, XRD, and neutron diffraction. Thereby a rhombohedral R3c phase with domain-like morphology is embedded in a "weakly-polar" tetragonal P4bm matrix phase [14].
- An electric field-induced phase transformation in the ternary system $(Bi_{1/2}Na_{1/2}TiO_3)_{1-x-y}$–$(BaTiO_3)_x$–$(K_{0.5}Na_{0.5}NbO_3)_y$ from tetragonal P4bm to rhombohedral R3c phase was verified by means of in situ electron microscopy [16] and neutron-diffraction experiments [49].

Acknowledgements We thank Lars Riekehr for TEM sample preparation, used for the conventional microscopic studies. Jürgen Rödel and Ian Reaney are thanked for helpful discussions, Xiaoli Tan for providing an opportunity to conduct the in situ electric field TEM experiments at the Department of Materials Science and Engineering, Iowa State University, Ames. X-ray and neutron experiments were performed at the Swiss Light Source, Paul Scherrer Institute (Villingen, Switzerland) and the research reactor Heinz Maier-Leibnitz, FRM-II (Garching near Munich, Germany), respectively. Special thanks to Antonio Cervellino, supporting the experiments at SLS. Financial support of the DFG within the SFB 595 "Electrical Fatigue in Functional Materials" and the BMBF (Bundesministerium für Bildung und Forschung) project grant No. 05K10ODA is gratefully acknowledged.

References

1. EU-Directive (2003) Off J Eur Union 46(L37):19
2. EU-Directive (2003) Off J Eur Union 46(L37):24
3. Saito Y, Takao H, Tani T, Nonoyama T, Takatori K, Homma T, Nagaya T, Nakamura M (2004) Nature 432(4):84
4. Maeder MD, Damjanovic D, Setter N (2004) J Electroceram 13:385
5. Li Y, Chen W, Xu Q, Zhou J (2005) J Mater Sci 40:3625. doi:10.1007/s10853-005-0716-6
6. Takenaka T, Nagata H, Hiruma Y, Yoshii Y, Matumoto K (2007) J Electroceram 19:259
7. Zhang S, Xia R, Shrout TR (2007) J Electroceram 19:251
8. Panda PK (2009) J Mater Sci 44:5049. doi:10.1007/s10853-009-3643-0
9. Xiao DQ, Wu JG, Wu L, Zhu JG, Yu P, Lin DM, Liao YW, Sun Y (2009) J Mater Sci 44:5408. doi:10.1007/s10853-009-3543-3
10. Lin D, Kwok KW (2009) J Mater Sci 44:4953. doi:10.1007/s10853-009-3756-5
11. Xu G, Yang D, Chen K, Payne DA, Carroll JF III (2010) J Electroceram 24:226
12. Damjanovic D, Klein N, Li J, Porokhonskyy V (2010) Funct Mater Lett 3(1):5

13. Zhang S-T, Kounga AB, Aulbach E, Ehrenberg H, Rödel J (2007) Appl Phys Lett 91:112906
14. Schmitt LA, Kleebe H-J (2010) Funct Mater Lett 3(1):55
15. Schmitt LA, Hinterstein M, Kleebe H-J, Fuess H (2010) J Appl Crystallogr 43:805
16. Kling J, Hayn S, Schmitt LA, Gröting M, Kleebe H-J, Albe K (2010) J Appl Phys 107:114113
17. Patterson BD, Abela R, Auderset H, Chen Q, Fauth F, Gozzo F, Ingold G, Kuehne H, Lange M, Maden D, Meister D, Pattison P, Schmidt T, Schmitt B, Schulze-Briese C, Shi M, Stampanoni M, Willmott PR (2005) Nucl Instr Methods Phys Res A 540:42
18. Bergamaschi A, Cervellino A, Dinapoli R, Gozzo F, Henrich B, Johnson I, Kraft P, Mozzanica A, Schmitt B, Shi X (2010) J Synchrotron Rad 17:653
19. Hoelzel M, Senyshyn A, Gilles R, Boysen H, Fuess H (2007) Neutron News 18:23
20. Roisnel T, Rodriguez-Carvajal J (2001) Mater Sci Forum 118:378
21. Thompson P, Cox DE, Hastings JB (1987) J Appl Crystallogr 20:79
22. Jones GO, Thomas PA (2000) Acta Crystallogr B56:426
23. Jones GO, Thomas PA (2002) Acta Crystallogr B58:168
24. Dorcet V, Trolliard G (2008) Acta Mater 56:1753
25. Dorcet V, Trolliard G, Boullay P (2008) Chem Mater 20:5061
26. Glazer M (1975) Acta Crystallogr A31:756
27. Trolliard G, Dorcet V (2008) Chem Mater 20:5074
28. Gorfman S, Thomas PA (2010) J Appl Crystallogr 43:1409
29. Kreisel J, Bouvier P, Dkhil B, Thomas PA, Glazer AM, Wlberry R, Chaabane B, Mezouar (2003) Phys Rev B68:014113
30. Cordero F, Cracium F, Trequattrini F, Mercadelli E, Galassi C (2010) Phys Rev B81:144124
31. Pronin IP, Syrnikov PP, Isupov VA, Egorov VM, Zaitseva NV (1980) Ferroelectrics 25:395
32. Takenaka T, Maruyama K, Sakata K (1991) Jpn J Appl Phys 30(9B):2236
33. Ge W, Liu H, Zhao X, Pan X, He T, Lin D, Xu H, Luo H (2008) J Alloys Compd 456:503
34. Rödel J, Jo W, Seifert KTP, Anton E-M, Granzow T, Damjanovic D (2009) J Am Ceram Soc 92(6):1153
35. Tai CW, Choy SH, Chan HL (2008) J Am Ceram Soc 91(10): 3335
36. Ge W, Cao H, Li J, Viehland D, Zhang Q, Luo H (2009) Appl Phys Lett 95:162903
37. Tai CW, Lereah Y (2009) Appl Phys Lett 95(6):062901
38. Zhang S-T, Kounga AB, Aulbach E, Jo W, Granzow T, Ehrenberg H, Rödel J (2008) J Appl Phys 103:034108
39. Zhang S-T, Kounga AB, Aulbach E, Deng Y (2008) J Am Ceram Soc 91(12):39503954
40. Zhang S-T, Kounga AB, Aulbach E, Granzow T, Jo W, Kleebe H-J, Rödel J (2008) J Appl Phys 103:034107
41. Kling J, Tan X, Jo W, Kleebe H-J, Fuess H, Rödel J (2010) J Am Ceram Soc 93(9):2452
42. Ma C, Tan X (2010) Solid State Commun 150:1497
43. Ranjan R, Dviwedi A (2005) Solid State Commun 135:394
44. Wylie-Van Eerd B, Damjanovic D, Klein N, Setter N, Trodahl J (2010) Phys Rev B82:104112
45. Reaney IM, Colla EL, Setter N (1994) Jpn J Appl Phys 33:3984
46. Soukhojak AN, Wang H, Farrey GW, Chiang Y-M (2000) J Phys Chem Solids 61:301
47. Park S-E, Chung S-J, Kim I-T (1996) J Am Ceram Soc 79(5): 1290
48. Jo W, Granzow T, Aulbach E, Rödel J, Damjanovic D (2009) J Appl Phys 105:094102
49. Hinterstein M, Knapp M, Hölzel M, Jo W, Cervellino A, Ehrenberg H, Fuess H (2010) J Appl Crystallogr 43:1314
50. Tan X, He H, Shang J-K (2005) J Mater Res 20:1641